INTERNATIONAL JOURNAL FOR NUMERICAL METHODS IN FLUIDS
Int. J. Numer. Meth. Fluids 2003; **41**:823–840 (DOI: 10.1002/fld.467)

Rotary oscillations of axi-symmetric bodies in an axi-symmetric viscous flow with slip: Numerical solutions for sphere and spheroids

P. Tekasakul[1,*,†] and S. K. Loyalka[2,‡]

[1] *Department of Mechanical Engineering, Faculty of Engineering, Thammasat University, Rangsit Campus Klong Luang, Pathum Thani 12121, Thailand*
[2] *Particulate Systems Research Center and Nuclear, Chemical, and Mechanical & Aerospace Engineering Departments, University of Missouri-Columbia, Columbia, MO 65211, U.S.A.*

SUMMARY

Rotary oscillations of several axi-symmetric bodies in axi-symmetric viscous flows with slip are investigated. A numerical method based on the Green's function technique is used wherein the relevant Helmholtz equation, as obtained from the unsteady Stokes equation, is converted into a surface integral equation. The technique is benchmarked against a known analytical solution, and accurate numerical results for local stress and torque on spheres and spheroids as function of the frequency parameter and the slip coefficients are obtained. It is found that in all cases, slip reduces stress and torque, and increasingly so with the increasing frequency parameter. The method discussed here can be potentially extended to the realistic case of an oscillating disk viscometer. Copyright © 2003 John Wiley & Sons, Ltd.

KEY WORDS: unsteady Stokes equation; oscillation; slip; axi-symmetric

1. INTRODUCTION

There have been several studies of oscillations of axi-symmetric bodies in axi-symmetric, viscous, incompressible flow at low Reynolds number with no-slip boundary conditions. Two important modes of oscillation involved the translational, in which the body performing oscillation displaces the fluid around the body, and the rotary, in which the body performing oscillation does not displace the fluid. Details of translational oscillation studies can be found in the literature [1–14]. The problem for the oscillation with small amplitude where the

* Correspondence to: P. Tekasakul, Department of Mechanical Engineering, Faculty of Engineering, Prince of Songkla University, Hat Yai, Songkla 90112, Thailand.
† E-mail: tekasakul@me.psu.ac.th
‡ E-mail: loyalkas@missouri.edu

Contract grant/sponsor: Thailand Research Fund; contract grant number: PDF/32/2541

Received March 2002
Accepted 15 July 2002

Reynolds number is very small arises from the principle that involves the solutions to the unsteady Stokes equations [15, 16],

$$\lambda^2 \frac{\partial \mathbf{u}}{\partial \tau} = -\nabla p + \nabla^2 \mathbf{u} \tag{1}$$

where $\lambda^2 = \omega a^2/v$ is the dimensionless frequency parameter. Here, a is the characteristic length of the body and ω is the frequency of oscillation, $v = \mu/\rho$ is the kinematic viscosity. Note that, μ is the dynamic viscosity and ρ is the mass density of the fluid.

The most notable application of rotary oscillations of axi-symmetric bodies is the oscillating cylindrical disk viscometer that has been used extensively in measurements of fluid viscosity. Moreover, rotary oscillations of a body in a fluid are of interest in studies of Brownian motion of particles, ultrasonics, and electroacoustics. The analytical solutions to the oscillation problem are limited to certain bodies with simple geometries. Some approximations are employed for more complicated bodies in order to facilitate analytical solutions. Recently, Tekasakul *et al.* [15] have solved the problem of several axi-symmetric bodies numerically from the unsteady Stokes equations for no-slip boundary conditions, and Zhang and Stone [16] have provided a range of useful solutions for bodies in several modes of rotation. These authors reported results for local stresses and torques on the bodies. Comparison showed that the accuracy of the numerical method was excellent. When the body dimension is only about an order of magnitude larger than molecular mean free path of the fluid, one must, however, consider fluid slip at the surface. The previous works [17–22], as it turns out, have emphasized the problem with no-slip boundary conditions with a few exceptions. MacWood [23, 24] obtained an approximate solution for a thin cylindrical disk with slip conditions (used in oscillating disk viscometer) by use of edge correction where some accuracy was lost. Shah [25] obtained slip solutions for some simple geometries in Laplace transform domain.

The slip at boundaries occurs when the Knudsen number (Kn) is in the order of 0.1. The Knudsen number is defined as the ratio of molecular mean free path of the medium (λ_g) and the characteristic length of the body (a), i.e. $Kn = \lambda_g/a$. The flow regimes classified by the Knudsen numbers include the free molecular ($Kn \gg 1$), the transition ($Kn \sim 1$), the slip ($Kn \sim 0.1$), and the continuum flow regime ($Kn \ll 1$). The molecular mean free path of the gas medium is defined as

$$\lambda_g = \frac{\mu}{p}\left(\frac{2kT}{m}\right)^{1/2}$$

where μ is the dynamic viscosity, p is the pressure, k is the Boltzmann's constant, T is the temperature, and m is the mass of the medium. The slip boundary condition at the surface of a body involves both the molecular mean free path and the slip coefficient, c_m, which can be represented quite accurately (error of 1%), by [26]

$$c_m = \frac{2-\alpha}{\alpha}\left[(1-\alpha)\frac{\pi^{1/2}}{2} + \alpha\zeta(1)\right]$$

where α is the momentum accommodation coefficient, and $\zeta(1)$, corresponding to $\alpha = 1$, has a value between 0.9875 and 1.02, depending on the nature of the gaseous intermolecular interaction. If $\zeta(1)$ is replaced by $\sqrt{\pi}/2$, the above equation becomes Maxwell's relation [27]. The slip becomes of greater significance as the pressure decreases below atmospheric, particularly

for the value of $Kn \sim 0.1$. For a slip flow, Navier–Stokes equations, and, hence, the unsteady Stokes equations are applicable when used with slip boundary conditions. Maxwell [27] defined the concept of the slip velocity by expressing the (asymptotic) surface velocity in terms of the (asymptotic) velocity gradient at the surface. Note that in a free molecular flow, solutions to the Boltzmann equations are needed, and the Navier–Stokes equations with slip do not suffice.

While solutions of the Navier–Stokes equation with slip conditions are of substantial interest for gases, recently it has been noted that slip conditions are of interest for liquids as well, particularly with respect to micro and nanofuidic conditions. For example, Barrat and Bocquet [28] have used molecular dynamics to compute slip for liquids, and Hervet and Leger [29] have measured slip for hexadecane on several modified sapphire surfaces using a rotating disk.

In this paper, we investigate calculations of local stresses and, hence, torques on axi-symmetric bodies performing rotary oscillation in an unbounded fluid medium and in viscous flow with slip boundary condition. The geometries of our interest are sphere, oblate spheroid and prolate spheroid. The numerical technique is based on that used by Tekasakul *et al.* [15]. The results of this paper are of interest for oscillating bodies in gases as well as liquids.

In the next section, the problem is described. In Section 3, analytical solutions for a sphere with constant slip on the surface are obtained from the technique employing the solutions from the no-slip case. In Section 4, numerical procedure for this problem is discussed and solution technique is outlined. In Section 5, numerical results and available analytical results for local stresses and torques for a sphere, an oblate spheroid and a prolate spheroid are presented. We discuss and conclude the present work in Section 6, together with suggestions for possible future work.

2. STATEMENT OF THE PROBLEM

We consider an axi-symmetric body (Figure 1) with a characteristic length, a, oscillating with frequency, ω, about its axis of symmetry (defined as the z-direction) in an unbounded gas with kinematic viscosity, ν, slip coefficient, c_m, and molecular mean free path, λ_g. The angular velocity of the oscillating body is given by $\Omega\cos(\omega t)$. The dimensionless unsteady Stokes' equation for a time-dependent, ϕ-component velocity as obtained from Equation (1), can be written as [15]

$$\lambda^2 \frac{\partial \hat{u}_\phi}{\partial \tau} = \left(\frac{\partial^2}{\partial \varpi^2} + \frac{1}{\varpi}\frac{\partial}{\partial \varpi} - \frac{1}{\varpi^2} + \frac{\partial^2}{\partial z^2} \right) \hat{u}_\phi \tag{2}$$

Here ϖ is the radial direction perpendicular to the z-axis as shown in Figure 1. The slip boundary condition at the body surface is

$$\hat{u}_\phi(\mathbf{r}_s) = \varpi_s \exp(\mathrm{i}\tau) + (c_m \lambda_g)\hat{\sigma}(\mathbf{r}_s) \tag{3}$$

while, far away from the body,

$$\lim_{\mathbf{r}\to\infty} \hat{u}_\phi(\mathbf{r}) = 0 \tag{4}$$

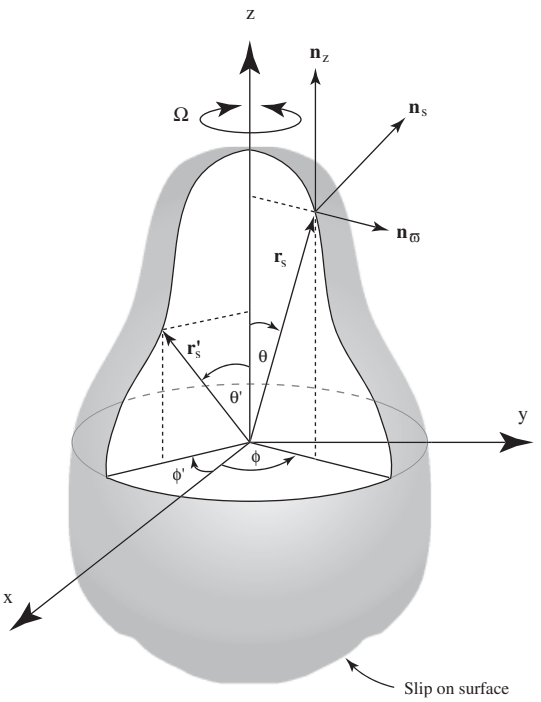

Figure 1. The co-ordinate system used in the present work for a general axi-symmetric body oscillating in an unbounded fluid with slip.

Here $\hat{\sigma}(\mathbf{r}_s)$ is the dimensionless time-dependent local stress. The length, time, velocity, and pressure are non-dimensionalized in terms of a, ω^{-1}, $U = |\Omega|a = \Omega a$, and $\mu U/a$, respectively. For a sphere, the characteristic length, a, is a radius whereas for prolate and oblate spheroids the equatorial radii are used. The solution is assumed to be of the form:

$$\hat{u}_\phi(\varpi, z, \tau) = \exp(\mathrm{i}\tau) u_\phi(\varpi, z) \tag{5}$$

Applying the Jeffery transformation [30]:

$$w(\varpi, z, \phi) = u_\phi(\varpi, z)\cos(\phi)$$

and following the manipulation of Tekasakul *et al.* [15], we have:

$$\nabla^2 w = \left(\frac{\partial^2}{\partial \varpi^2} + \frac{1}{\varpi}\frac{\partial}{\partial \varpi} - \frac{1}{\varpi^2} + \frac{\partial^2}{\partial z^2} \right) u_\phi \cos(\phi) \tag{6}$$

which leads to the Helmholtz equation:

$$(\nabla^2 + k^2) w = 0 \tag{7}$$

The slip boundary condition at the surface now becomes

$$w(\mathbf{r}_s) = [\varpi_s + (c_m \lambda_g)\sigma(\mathbf{r}_s)]\cos(\phi_s) \tag{8}$$

and the limiting condition of the fluid far away from the body is

$$\lim_{\mathbf{r}\to\infty} w(\mathbf{r}) = 0 \tag{9}$$

Here $\lambda^2 = \omega a^2/\nu$ is the dimensionless frequency parameter and $k^2 = -\mathrm{i}\lambda^2$ is the dimensionless complex-valued frequency parameter. The dimensionless, time-independent local stress is defined as

$$\sigma(\zeta) = \varpi \frac{\partial}{\partial n}\left(\frac{u_\phi}{\varpi}\right) \tag{10}$$

while the dimensionless, time-independent torque on the body can be evaluated from

$$T = 2\pi \int_c \varpi^2 \sigma(\zeta)\, \mathrm{d}s \tag{11}$$

Here, ζ is a co-ordinate specifying a point on the meridian contour of the body for which $-1 \leqslant \zeta \leqslant 1$. Note that the dimensionless, time-independent torque has been non-dimensionalized by $\Omega\mu a^3$ and the transient term $\exp(\mathrm{i}\tau)$ has been dropped.

3. ANALYTICAL SOLUTIONS FOR CONSTANT SLIP

The solution of an oscillating sphere in an infinite fluid medium with slip can be obtained from the solution of the oscillation sphere with no-slip. We consider two separate problems, one with no-slip and the other with non-zero constant slip, simultaneously. For the no-slip case, Equations (7)–(9) with $c_m\lambda_g = 0$, can be written as

$$Lu_{\phi 1} = 0 \tag{12}$$

The no-slip boundary condition at the surface of the sphere becomes

$$u_{\phi 1} = \sin\theta \tag{13}$$

where θ is the polar angle and far away from the sphere:

$$\lim_{\mathbf{r}\to\infty} u_{\phi 1} = 0 \tag{14}$$

For the constant-slip, the problem can be written as

$$Lu_{\phi 2} = 0 \tag{15}$$

The slip boundary condition at the surface of the sphere is

$$u_{\phi 2} = \sin\theta + c_2 \sin\theta = (1 + c_2)\sin\theta \tag{16}$$

and the limiting condition of the fluid far away from the sphere is

$$u_{\phi 2} = 0 \tag{17}$$

where ϕ_s and c_2 are constants, subscripts 1 and 2 represent the no-slip and constant slip cases, respectively, and the operator L is

$$L=\left(\frac{\partial^2}{\partial\varpi^2}+\frac{1}{\varpi}\frac{\partial}{\partial\varpi}-\frac{1}{\varpi^2}+\frac{\partial^2}{\partial z^2}\right)+k^2$$

Substituting $u_{\phi 2}=(1+c_2)u_{\phi 1}$ into Equations (15)–(17), the slip problem becomes the no-slip problem. Therefore the relation

$$u_{\phi 2}=(1+c_2)u_{\phi 1} \tag{18}$$

is the solution for the slip problem.

From Equation (8) for the slip case, the constant, c_2, can be written as

$$c_2=\frac{(c_m\lambda_g)}{\sin\theta}\sigma_2=\frac{(c_m\lambda_g)}{\sin\theta}\varpi\frac{\partial}{\partial n}\left(\frac{u_{\phi 2}}{\varpi}\right) \tag{19}$$

Now dividing Equation (18) by ϖ, differentiating the resulting expressions with respect to the normal direction, and multiplying by ϖ, we get

$$\varpi\frac{\partial}{\partial n}\left(\frac{u_{\phi 2}}{\varpi}\right)=(1+c_2)\varpi\frac{\partial}{\partial n}\left(\frac{u_{\phi 1}}{\varpi}\right) \tag{20}$$

that is,

$$\sigma_2=\left(1+\frac{c_m\lambda_g}{\sin\theta}\sigma_2\right)\sigma_1 \tag{21}$$

And we get,

$$\sigma_2=\frac{\sigma_1}{1-\sigma_1(c_m\lambda_g)/\sin\theta} \tag{22}$$

The above equation shows that the stress on the oscillating sphere for the constant-slip case (σ_2) can be determined from the knowledge of the stress for the no-slip case (σ_1).

Since the local stress for the no-slip case is [15, 17]

$$\sigma_{\text{zero-slip}}=\sigma_1=-\left[3-\frac{k^2}{1+\mathrm{i}k}\right]\sin\theta \tag{23}$$

the local stress for the slip case becomes

$$\sigma_{\text{slip}}=\sigma_2=\frac{-\left[3-\dfrac{k^2}{1+\mathrm{i}k}\right]\sin\theta}{1+(c_m\lambda_g)\left[3-\dfrac{k^2}{1+\mathrm{i}k}\right]} \tag{24}$$

Torque on the sphere can then be evaluated straightforwardly from

$$
\begin{aligned}
T &= 2\pi \int_c \varpi^2 \sigma \, \mathrm{d}s \\
&= 2\pi \int_0^{\pi} \sin^2\theta \left\{ \frac{-\left[3 - \dfrac{k^2}{1+\mathrm{i}k}\right] \sin\theta}{1 + (c_m\lambda_g)\left[3 - \dfrac{k^2}{1+\mathrm{i}k}\right]} \right\} \mathrm{d}\theta \\
&= -\frac{8}{3}\pi \frac{3 - \dfrac{k^2}{1+\mathrm{i}k}}{1 + (c_m\lambda_g)\left[3 - \dfrac{k^2}{1+\mathrm{i}k}\right]}
\end{aligned} \tag{25}
$$

However, these simple forms of relationship do not appear to hold in general for spheroids, for which even the no-slip case leads to complicated eigenfunction expansions.

4. NUMERICAL SOLUTIONS

The numerical method used in the present work is based on the Green's function approach in which for this problem, it can be defined by

$$(\nabla^2 + k^2)\psi(\mathbf{r}, \mathbf{r}') = -4\pi\delta(\mathbf{r} - \mathbf{r}') \tag{26}$$

such that

$$\psi(\mathbf{r}, \mathbf{r}') = \frac{\exp(-\mathrm{i}k|\mathbf{r} - \mathbf{r}'|)}{|\mathbf{r} - \mathbf{r}'|} \tag{27}$$

Following the procedure of Tekasakul *et al.* [15] [see their Equations (23)–(26)], and applying the slip boundary condition, the problem becomes

$$
\begin{aligned}
&-\int \left(\psi(\mathbf{r}_s, \mathbf{r}_s') \left\{ \cos(\phi')\sigma(\mathbf{r}_s') + \left[\frac{(c_m\lambda_g)\sigma(\mathbf{r}_s')}{\varpi_s'} \right] \frac{\partial}{\partial n_s'} [\varpi_s' \cos(\phi')] \right\} \right. \\
&\qquad \left. -[(c_m\lambda_g)\sigma(\mathbf{r}_s')] \cos(\phi') \frac{\partial \psi(\mathbf{r}_s, \mathbf{r}_s')}{\partial n_s'} \right) \mathrm{d}\mathbf{r}_s' \\
&= 2\pi[\varpi_s + (c_m\lambda_g)\sigma(\mathbf{r}_s)] \cos(\phi) \\
&\quad + \int \left[\psi(\mathbf{r}_s, \mathbf{r}_s') \frac{\partial}{\partial n_s'} [\varpi_s' \cos(\phi')] - \varpi_s' \cos(\phi') \frac{\partial \psi(\mathbf{r}_s, \mathbf{r}_s')}{\partial n_s'} \right] \mathrm{d}\mathbf{r}_s'
\end{aligned} \tag{28}
$$

Using Green's second identity and

$$\nabla^2_{\mathbf{r}'} \varpi'_s \cos(\phi'_s) = 0 \tag{29}$$

Equation (28) becomes

$$\begin{aligned} &- \int \left\{ \psi(\mathbf{r}_s, \mathbf{r}'_s) \cos(\phi'_s) \sigma(\zeta') \left[1 + \frac{(c_m \lambda_g)}{\varpi'_s} \frac{\partial \varpi'_s}{\partial n'_s} \right] \right\} J'_s \, \mathrm{d}\phi'_s \, \mathrm{d}\zeta' \\ &\quad + \int \left\{ [(c_m \lambda_g) \cos(\phi') \sigma_1(\zeta')] \frac{\partial \psi(\mathbf{r}_s, \mathbf{r}'_s)}{\partial n'_s} \right\} J'_s \, \mathrm{d}\phi'_s \, \mathrm{d}\zeta' \\ &= 2\pi (c_m \lambda_g) \sigma(\mathbf{r}_s) \cos(\phi) - k^2 \int \psi(\mathbf{r}_s, \mathbf{r}'_s) \varpi'_s \cos(\phi'_s) J'_s \, \mathrm{d}\phi' \, \mathrm{d}\zeta' \end{aligned} \tag{30}$$

as $\mathrm{d}\mathbf{r}_s = J \, \mathrm{d}\zeta \, \mathrm{d}\phi$, where J is the Jacobian for the integration.

We define,

$$f = 1 + \frac{(c_m \lambda_g)}{\varpi'_s} \frac{\partial \varpi'_s}{\partial n'_s}$$

$$K = \frac{J'_s}{\cos(\phi)} \left[\int \psi(\mathbf{r}_s, \mathbf{r}'_s) \cos(\phi') \, \mathrm{d}\phi' \right]$$

$$H = \frac{J'_s}{\cos \phi_s} \left[\int \frac{\partial \psi(\mathbf{r}_s, \mathbf{r}'_s)}{\partial n'_s} \cos(\phi') \, \mathrm{d}\phi' \right]$$

and

$$\Psi = \frac{J'_s}{\cos \phi_s} \left[\int \psi(\mathbf{r}_s, \mathbf{r}'_s) \varpi'_s \cos(\phi') \, \mathrm{d}\phi' \, \mathrm{d}\zeta' \right]$$

Whence Equation (30) can be written as

$$\int L(\zeta, \zeta') \, \sigma(\zeta') \, \mathrm{d}\zeta' = -k^2 \Psi(\zeta, \zeta') + 2\pi (c_m \lambda_g) \sigma(\zeta) \tag{31}$$

where

$$L(\zeta, \zeta') = -f(\zeta') K(\zeta, \zeta') + (c_m \lambda_g) H(\zeta, \zeta') \tag{32}$$

Equation (31) is a Fredholm integral equation of the second kind. Applying the singularity subtraction technique, the above equation becomes

$$g(\zeta)\sigma(\zeta) + \int L(\zeta, \zeta') \, [\sigma(\zeta') - \sigma(\zeta)] \, \mathrm{d}\zeta' = -k^2 \Psi(\zeta, \zeta') + 2\pi (c_m \lambda_g) \sigma(\zeta)$$

or

$$[g(\zeta) - 2\pi(c_m\lambda_g)]\sigma(\zeta) + \int L(\zeta,\zeta')\,[\sigma(\zeta') - \sigma(\zeta)]\,\mathrm{d}\zeta' = -k^2\Psi(\zeta,\zeta') \tag{33}$$

where

$$g(\zeta) = \int_{-1}^{1} L(\zeta,\zeta')\,\mathrm{d}\zeta' \tag{34}$$

The integrals in Equation (33) are converted to summations by the use of Gaussian quadratures. Together with collocation at the nodal points of the quadrature, Equation (33) then reduces to a system of linear algebraic equations. The stress, $\sigma(\zeta)$, is determined at the nodal points of the quadrature. The total torque can then be determined from the stresses using Equations (10) and (11).

4.1. Determination of f

For the case of a sphere, we can write, $z = r\cos\theta$, $\varpi = r\sin\theta$, and

$$\frac{1}{\varpi_s}\frac{\partial\varpi_s}{\partial n_s} = \frac{1}{\varpi_s}\left.\frac{\partial\varpi}{\partial r}\right|_{r=1} = 1$$

then

$$f = 1 + (c_m\lambda_g) \tag{35}$$

For spheroids with the geometries shown in Figure 2, in which $z = c\lambda\zeta$, $\varpi = c[(1+\lambda^2)(1-\zeta^2)]^{1/2}$, we have

$$c^2 = \begin{cases} A^{-2} - 1 & \text{Prolate spheroid} \\ 1 - A^{-2} & \text{Oblate spheroid} \end{cases}$$

$$\lambda_0 = \frac{b}{c} \quad \text{at surface}$$

$$h_\lambda = \frac{1}{c}\left(\frac{1+\lambda^2}{\zeta^2+\lambda^2}\right)^{1/2}$$

and

$$\frac{1}{\varpi_s}\frac{\partial\varpi_s}{\partial n_s} = \frac{1}{\varpi_s}h_{\lambda_0}\left.\frac{\partial\varpi}{\partial\lambda}\right|_{\lambda_0} = \frac{\lambda_0}{c[(1+\lambda_0^2)(\zeta^2+\lambda_0^2)]^{1/2}}$$

Hence

$$f = 1 + \frac{(c_m\lambda_g)}{c}\cdot\frac{\lambda_0}{[(1+\lambda_0^2)(\zeta^2+\lambda_0^2)]^{1/2}} \tag{36}$$

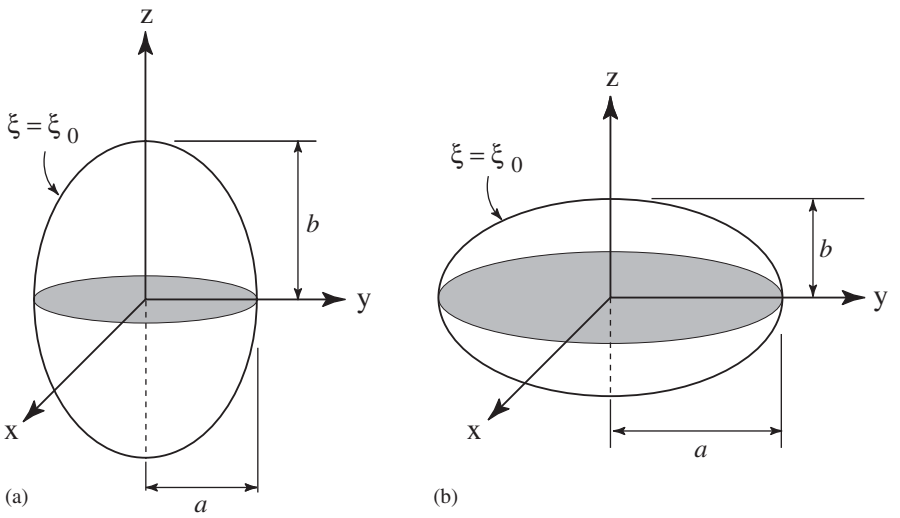

Figure 2. The spheroidal geometries that are considered in this work. (a) Prolate spheroidal co-ordinates. (b) Oblate spheroidal co-ordinates. In both cases, the aspect ratio is $A = a/b$.

4.2. Determination of K

The expression of K can be written as [15]

$$K(\zeta,\zeta') = \frac{J_s'}{\cos(\phi)} \int \psi(\mathbf{r}_s,\mathbf{r}_s') \cos(\phi')\,\mathrm{d}\phi' = K_L(\zeta,\zeta') + K_H(\zeta,\zeta') \tag{37}$$

where

$$K_L(\zeta,\zeta') = \frac{J_s'}{\cos(\phi)} \int \frac{\cos(\phi')}{|\mathbf{r}_s' - \mathbf{r}_s|}\,\mathrm{d}\phi' = \frac{2J_s'}{\sqrt{\varpi_s\varpi_s'}}\, Q_{1/2}(\gamma) \tag{38}$$

and

$$K_H(\zeta,\zeta') = \frac{J_s'}{\cos(\phi)} \int \frac{\exp(-\mathrm{i}k|\mathbf{r}_s' - \mathbf{r}_s|) - 1}{|\mathbf{r}_s' - \mathbf{r}_s|} \cos(\phi')\,\mathrm{d}\phi' = \frac{J_s'}{\cos(\phi)} \int_0^{2\pi} \frac{\exp(-\mathrm{i}k[2\varpi_s\varpi_s'(\gamma - \cos(\phi - \phi'))]^{1/2}) - 1}{[2\varpi_s\varpi_s'(\gamma - \cos(\phi - \phi'))]^{1/2}} \cos(\phi')\,\mathrm{d}\phi' \tag{39}$$

Here, $Q_{1/2}(\gamma)$ is an Associated Legendre function of fractional order with the argument

$$\gamma = 1 + \frac{\beta}{2\varpi_s\varpi_s'}$$

in which

$$\beta = (\varpi_s' - \varpi_s)^2 + (z_s' - z_s)^2$$

4.3. Determination of H

The expression of H can be written as

$$H = \frac{J_s'}{\cos(\phi)} \left[\int \frac{\partial \psi(\mathbf{r}_s, \mathbf{r}_s')}{\partial n_s'} \cos(\phi_s') \, \mathrm{d}\phi_s' \right]$$

Since

$$\psi(\mathbf{r}_s, \mathbf{r}_s') = \frac{\exp(-\mathrm{i}kt)}{t}$$

and $\mathbf{t} = |\mathbf{r}_s - \mathbf{r}_s'|$, we have:

$$\begin{aligned} \frac{\partial \psi(\mathbf{r}_s, \mathbf{r}_s')}{\partial n_s'} &= (1 + \mathrm{i}kt) \exp(-\mathrm{i}kt) \frac{\partial}{\partial n'} \left(\frac{1}{t} \right) \\ &= (1 + \mathrm{i}kt) \exp(-\mathrm{i}kt) \left(- \frac{(\mathbf{r}_s' - \mathbf{r}_s) \cdot \mathbf{n}_{\text{outward}}'}{|\mathbf{r}_s - \mathbf{r}_s'|^3} \right) \end{aligned}$$

And thus, for spheroids in general (including sphere), we have

$$\begin{aligned} H(\zeta, \zeta') = -\frac{1}{\cos(\phi)} \frac{\varpi_s'}{A} \int_0^{2\pi} \{ &(1 + \mathrm{i}kt) \exp(-\mathrm{i}kt) [2\varpi_s \varpi_s' (\gamma - \cos(\phi - \phi'))]^{-3/2} \\ &\left[[z_s' - z_s] \frac{z_s'}{[A^{-2} - z_s'^2]^{1/2}} A + \varpi_s' - \varpi_s \cos(\phi - \phi') \right] \cos(\phi') \Big\} \, \mathrm{d}\phi' \end{aligned} \tag{40}$$

4.4. Determination of Ψ

From Tekasakul *et al.* [15], we have

$$\Psi(\zeta) \cos(\phi) = -\frac{4\pi}{k^2} (\varpi_s \cos(\phi)) - \int_{\substack{\text{inside} \\ \text{body}}} \frac{\exp(-\mathrm{i}k|\mathbf{r}' - \mathbf{r}_s|)}{|\mathbf{r}' - \mathbf{r}_s|} \varpi' \cos(\phi') \, \mathrm{d}\mathbf{r}' \tag{41}$$

For a sphere, this expression can be written as

$$\begin{aligned} \Psi(\zeta) \cos(\phi) = \frac{2\pi \varpi_s \cos(\phi)}{k^2} \Big\{ &-2 + \left(1 + \frac{\mathrm{i}}{k} \right) + \exp(-\mathrm{i}2k) \left(1 - \frac{\mathrm{i}}{k} \right) \\ &+ \frac{\mathrm{i}}{k} \left(1 + \frac{3}{k^2} \right) - \frac{\exp(-\mathrm{i}2k)}{k^3} (3\mathrm{i} - 6k - 5\mathrm{i}k^2 + 2k^3) \Big\} \end{aligned} \tag{42}$$

For a prolate spheroid, it becomes [31]

$$\begin{aligned}\Psi(\zeta)\cos(\phi) &= -\frac{4\pi}{k^2}[\varpi_s\cos(\phi)] - \frac{c^3}{2}\int_0^{\xi_0} d\xi' \int_0^{\pi} d\eta' \int_0^{2\pi} d\phi' \\ &\times \left\{ \frac{\exp(-ik[2\varpi_s\varpi_s'(\gamma-\cos(\phi-\phi'))]^{1/2})}{[2\varpi_s\varpi_s'(\gamma-\cos(\phi-\phi'))]^{1/2}} \right. \\ &\left. \times\, \varpi'\cos(\phi')[\cosh(2\xi')-\cos(2\eta')]\sinh(\xi')\sin(\eta') \right\} \end{aligned} \tag{43}$$

And finally, for an oblate spheroid, we have [31]

$$\begin{aligned}\Psi(\zeta)\cos(\phi) &= -\frac{4\pi}{k^2}[\varpi_s\cos(\phi)] - \frac{c^3}{2}\int_0^{\xi_0} d\xi' \int_0^{\pi} d\eta' \int_0^{2\pi} d\phi' \\ &\times \left\{ \frac{\exp(-ik[2\varpi_s\varpi_s'(\gamma-\cos(\phi-\phi'))]^{1/2})}{[2\varpi_s\varpi_s'(\gamma-\cos(\phi-\phi'))]^{1/2}} \right. \\ &\left. \times\varpi'\cos(\phi')[\cosh(2\xi')+\cos(2\eta')]\cosh(\xi')\sin(\eta') \right\} \end{aligned} \tag{44}$$

5. LOCAL STRESSES AND TORQUES

Our main goal in this paper is to study the effect of the slip on the local stress on the surface and torque exerted on an oscillating sphere and spheroids, and to assess the accuracy of a numerical technique. We have carried out numerical calculations using *Mathematica*® 4.0. We have benchmarked the accuracy of the method against known solution for a sphere. The results of this benchmarking are reported below and are followed by our results for the prolate and oblate spheroids.

Numerical results for the dimensionless time-independent torque (T) are presented as functions of the product of the slip coefficient and molecular mean free path ($c_m\lambda_g$) for the dimensionless frequency parameter (λ^2) between 0.01 to 100.0. Since $k^2 = -i\lambda^2$, only the positive root of k is used, i.e.:

$$k = +(1-i)\lambda/\sqrt{2} \tag{45}$$

The time-independent torque is obtained by dropping the term, $\exp(i\tau)$. The real part of torque is a component that varies in phase with body motion while the imaginary part is the out-of-phase component and then does not contribute to energy dissipation [16].

5.1. Sphere

Since the analytical solution for an oscillating sphere with slip can be obtained from the no-slip solution, we first benchmark the accuracy of the numerical method against the analytical solutions for a sphere for values of $c_m\lambda_g$ ranging from 0.001 to 0.1 and values of λ^2 ranging from 0.01 to 100.0. In these calculations, 20 point Gaussian quadratures were used for $\lambda^2 \leqslant 10.0$ and 30 point quadratures were used for $\lambda^2 = 100.0$. Both the torques and the local stresses on the sphere are calculated and compared to the corresponding analytical values.

Numerical results for the real and imaginary parts of the torque on a sphere are given in Figures 3(a) and 3(b), respectively. Analytical values for this sphere that have been determined from Equation (25) are also included for comparison. In general the agreement is very good. The numerical results differ from the analytical values by a maximum of 4%. In this section, values of λ^2 is displayed instead of k^2 since k^2 is complex. Torques increase with increasing λ^2, as expected [15]. As seen in Figures 3(a) and 3(b), the values of torques decrease as the slip term $c_m\lambda_g$ becomes greater. The decrease of the real part of torque ranges from 23% for $\lambda^2 = 0.01$ to 41% for $\lambda^2 = 100.0$, while, for the imaginary part, the decrease ranges from 41% for $\lambda^2 = 0.01$ to 76% for $\lambda^2 = 100.0$. It is obvious that the effect of slip is significant for the range considered ($0.001 \leqslant c_m\lambda_g \leqslant 0.1$) and becomes greater for an oscillation with higher frequency. Numerical results for the real and imaginary parts of the local stress on a sphere for which $\lambda^2 = 1.0$ have been obtained via our numerical technique and are compared with values calculated from Equation (24) in Figures 3(c) and 3(d), respectively. The agreement is generally very good with errors less than 1% over the entire range of ζ except for $c_m\lambda_g = 0.1$ where the error increases to about 5%.

The good agreement between the numerical and analytical values for the case of a sphere demonstrates that the order of quadrature used are appropriate. The errors are quite small for small values of λ^2 and increase noticeably only for the largest values of λ^2. The errors at large values of λ^2 are due to the relative thinness of the oscillatory viscous boundary layer which requires a higher number of Gaussian quadrature points for accurate modeling.

5.2. Prolate spheroid

Twenty-point Gaussian quadratures were also used in these calculations. Numerical results for the real and imaginary parts of the torque on a typical prolate spheroid with $A = 0.5$ are given in Figures 4(a) and 4(b), respectively. Tekasakul *et al.* [15] showed that for the prolate spheroid with the same aspect ratio, the no-slip torque increases as λ^2 increases. As shown in Figures 4(a) and 4(b), torque decreases as the slip term $c_m\lambda_g$ becomes greater, as in the case of the sphere. The decrease of the real part of torque ranges from 16% for $\lambda^2 = 0.01$ to 31% for $\lambda^2 = 100.0$, while, for the imaginary part, the decrease ranges from 35% for $\lambda^2 = 0.01$ to 72% for $\lambda^2 = 100.0$. The effect of slip for a prolate spheroid is similar to the case of a sphere in the previous section for the range considered ($0.001 \leqslant c_m\lambda_g \leqslant 0.1$). Numerical results for the real and imaginary parts of the local stress on the same prolate spheroid for which $\lambda^2 = 1.0$ are also shown in Figures 4(c) and 4(d), respectively. The results are similar to those of a sphere.

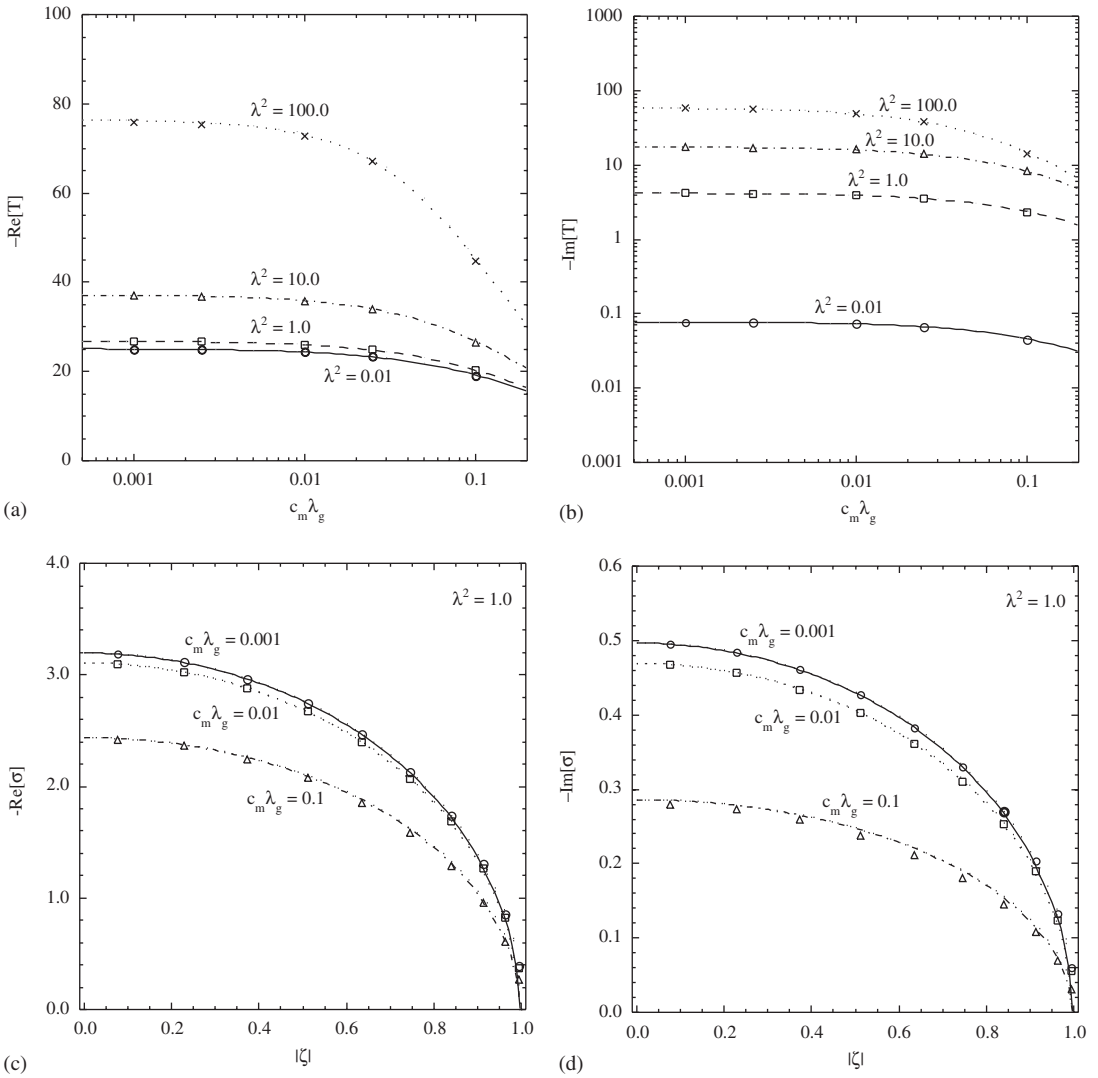

Figure 3. A comparison of the numerically determined torques and local stresses on a sphere with the corresponding values determined analytically. Symbols indicate numerical results while various lines indicate corresponding analytical results. (a) The real parts of the torques for $\lambda^2 = 0.01$–100.0. (b) The imaginary parts of the torques for $\lambda^2 = 0.01$–100.0. (c) The real parts of the local stresses for $\lambda^2 = 1.0$ and $c_m\lambda_g = 0.001$, 0.01, and 0.1. (d) The imaginary parts of the local stresses for $\lambda^2 = 1.0$ and $c_m\lambda_g = 0.001$, 0.01, and 0.1. The number of Gaussian quadrature points used in the numerical calculations was 20. Due to symmetry, only the stress values for the upper half of each body have been shown. Here, ζ is the co-ordinate that specifies points on the meridian contours of the bodies, and $\lambda^2 = \omega a^2/\nu$ is the dimensionless frequency parameter.

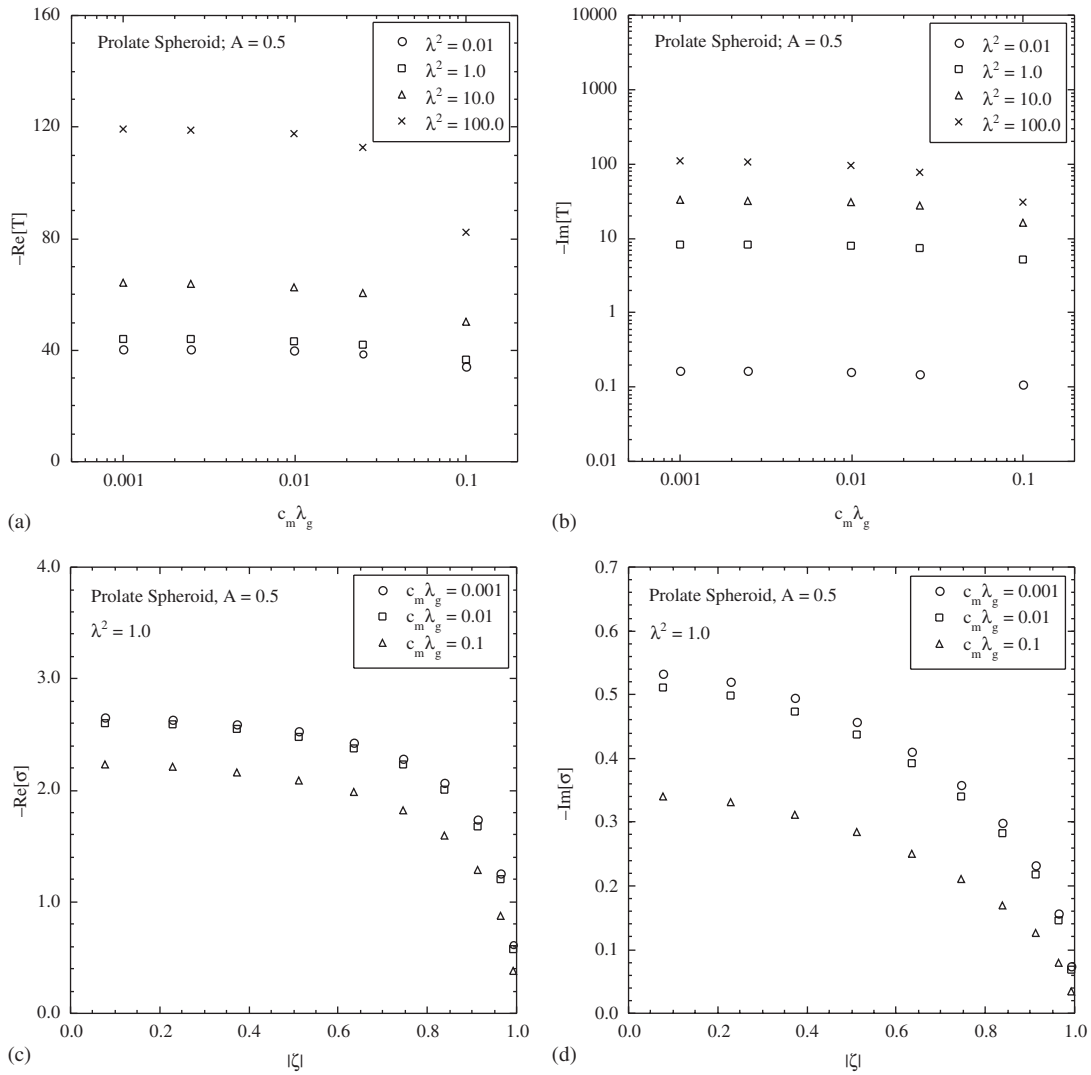

Figure 4. Numerical results for torques and local stresses on a prolate spheroid with $A = 0.5$. (a) The real parts of the torques for $\lambda^2 = 0.01$–100.0. (b) The imaginary parts of the torques for $\lambda^2 = 0.01$–100.0. (c) The real parts of the local stresses for $\lambda^2 = 1.0$ and $c_m\lambda_g = 0.001$, 0.01, and 0.1. (d) The imaginary parts of the local stresses for $\lambda^2 = 1.0$ and $c_m\lambda_g = 0.001$, 0.01, and 0.1. The number of Gaussian quadrature points used in the numerical calculations was 20.

5.3. *Oblate spheroid*

We used 20-point Gaussian quadratures in the calculation for an oblate spheroid also. Numerical results for the real and imaginary parts of the torque on a typical oblate spheroid with $A = 2.0$ are given in Figures 5(a) and 5(b), respectively. As also shown by Tekasakul *et al.* [15], the torque increases as λ^2 increases. The torque for the oblate spheroid decreases

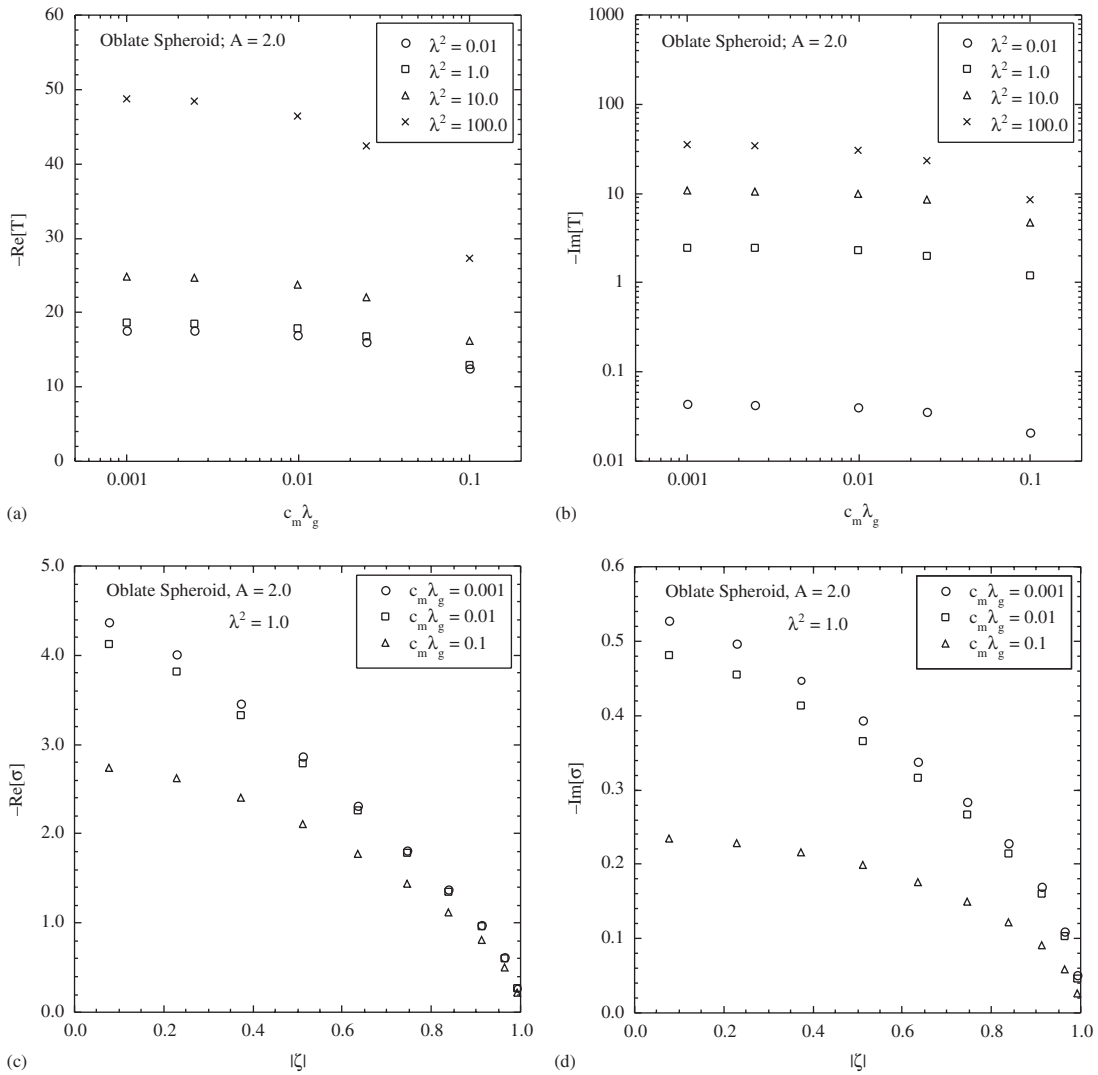

Figure 5. Numerical results for torques and local stresses on an oblate spheroid with $A = 2.0$. (a) The real parts of the torques for $\lambda^2 = 0.01$–100.0. (b) The imaginary parts of the torques for $\lambda^2 = 0.01$–100.0. (c) The real parts of the local stresses for $\lambda^2 = 1.0$ and $c_m\lambda_g = 0.001$, 0.01, and 0.1. (d) The imaginary parts of the local stresses for $\lambda^2 = 1.0$ and $c_m\lambda_g = 0.001$, 0.01, and 0.1. The number of Gaussian quadrature points used in the numerical calculations was 20.

as the slip term $c_m\lambda_g$ becomes greater, as in the case of the sphere and the prolate spheroid considered previously. The decrease of the real part of torque ranges from 29% for $\lambda^2 = 0.01$ to 44% for $\lambda^2 = 100.0$, while, for the imaginary part, the decrease ranges from 51% for $\lambda^2 = 0.01$ to 76% for $\lambda^2 = 100.0$. The effect of slip for an oblate spheroid is also similar to the case of a sphere and a prolate spheroid in the previous section for the range considered

($0.001 \leqslant c_m \lambda_g \leqslant 0.1$). Numerical results for the real and imaginary parts of the local stress on the same oblate spheroid for which $\lambda^2 = 1.0$ are shown in Figures 5(c) and 5(d), respectively. The results are similar to those of a sphere and a prolate spheroid.

6. DISCUSSIONS AND CONCLUSION

We have shown that the numerical technique, used in the calculations of torques and local stresses on axi-symmetric bodies undergoing slow rotary oscillations about their axes of symmetry in unbounded viscous fluids with slip, is accurate by benchmarking against exact solution for a sphere. The numerical results for spheres agree well (maximum error less than 4%) with the corresponding analytical values as shown in Figures 3(a)–3(d). The accuracy of the calculations can be improved for high oscillating frequency (λ^2) by increasing number of Gaussian quadrature points. In the present work, we have used 20-point quadrature throughout for the values of λ^2 as high as 100.0 except for the case of a sphere where the 30-point quadrature was used for the case of $\lambda^2 = 100.0$. In the range of slip we have studied ($0.001 \leqslant c_m \lambda_g \leqslant 0.1$), it is apparent that the increase of slip always lowers the values of torques and the effect is greater for higher value of λ^2. The reduction of torque due to the presence of slip at the body surface therefore shortens the period of oscillation of the bodies. The effect of slip for a typical prolate spheroid ($A = 0.5$) and a typical oblate spheroid ($A = 2.0$) were found to follow the same trend as in the case of a sphere.

This work is a continuing effort in the investigation for the complete solutions for the problem of axi-symmetric bodies undergoing rotary oscillation used previously in calculations of the torque on axi-symmetric bodies undergoing rotary oscillation in an unbounded fluid without slip on the surface of the bodies [15]. One of the most notable applications of rotary oscillation of an axi-symmetric body, as stated earlier, is the oscillating disk viscometer. We are planning to extend the work of this paper to viscometer in the near future, and this should facilitate the extraction of the velocity slip and tangential momentum accommodation coefficients also from the data in the same manner as has been accomplished by the use of spinning rotor gauge [32,33].

ACKNOWLEDGEMENTS

This research was supported by the Thailand Research Fund (TRF) through grant PDF/32/2541. We are thankful to Dr. R.V. Tompson for his critical reading and many helpful comments.

REFERENCES

1. Kanwal RP. Rotatory and longitudinal oscillations of axi-symmetric bodies in a viscous fluid. *The Quarterly Journal of Mechanics and Applied Mathematics* 1955; **8**:146–163.
2. Kanwal RP. Drag on an axially symmetric body vibrating slowly along its axis in a viscous fluid. *Journal of Fluid Mechanics* 1964; **19**:631–636.
3. William WE. A note on slow vibrations in a viscous fluid. *Journal of Fluid Mechanics* 1966; **25**:589–590.
4. Lawrence CJ, Weinbaum S. The force on an axisymmetric body in linearized, time-dependent motion: A new memory term. *Journal of Fluid Mechanics* 1986; **171**:209–218.
5. Lawrence CJ, Weinbaum S. The unsteady force on a body at low Reynolds number; the axisymmetric motion of a spheroid. *Journal of Fluid Mechanics* 1988; **189**:463–489.
6. Pozrikidis C. A study of linearized oscillatory flow past particles by the boundary-integral method. *Journal of Fluid Mechanics* 1989; **202**:17–41.

7. Pozrikidis C. A singularity method for unsteady linearized flow. *Physics of Fluids A* 1989; **1**:1508–1520.
8. Loewenberg M. Stokes resistance, added mass, Basset force for arbitrarily oriented, finite-length cylinders. *Physics of Fluids A* 1993; **5**:765–767.
9. Loewenberg M. The unsteady Stokes resistance of arbitrarily oriented, finite-length cylinders. *Physics of Fluids A* 1993; **5**:3004-3006.
10. Loewenberg M. Asymmetric, oscillatory motion of a finite-length cylinder: The macroscopic effect of particle edges. *Physics of Fluids A* 1994; **6**:1095–1107.
11. Loewenberg M. Axisymmetric unsteady Stokes flow past an oscillating finite-length cylinder. *Journal of Fluid Mechanics* 1994; **265**:265–288.
12. Davis AMJ. A hydrodynamic model of the oscillating screen viscometer. *Physics of Fluids A* 1993; **5**: 2095–2103.
13. Lovalenti PM, Brady JF. The hydrodynamic force on a rigid particle undergoing arbitrary time-dependent motion at small Reynolds number. *Journal of Fluid Mechanics* 1993; **256**:561–605.
14. Lovalenti PM, Brady JF. The force on a sphere in a uniform flow with small-amplitude oscillations at finite Reynolds number. *Journal of Fluid Mechanics* 1993; **256**:607–614.
15. Tekasakul P, Tompson RV, Loyalka SK. Rotatory oscillations of arbitrary axi-symmetric bodies in an axi-symmetric viscous flow: Numerical solutions. *Physics of Fluids* 1998; **10**:2797–2818.
16. Zhang W, Stone HA. Oscillatory motions of circular disks and near spheres in viscous flows. *Journal of Fluid Mechanics* 1998; **367**:329–358.
17. Lamb H. *Hydrodynamics* (6th edn). Dover: New York, 1932; pp. 642–644.
18. Kanwal RP. Note on slow rotation or rotary oscillation of axisymmetric bodies in hydrodynamics and magnetohydrodynamics. *Journal of Fluid Mechanics* 1970; **41**:721–726.
19. Kestin J, Persen LN. Slow oscillations of bodies of revolution in a viscous fluid. *Proceedings of the International Congress of Applied Mechanics* 1956; **9**:326–338.
20. Mariens P, van Paemel O. Theory and experimental verification of the oscillating disk method for viscosity measurements in fluids. *Applied Scientific Research A* 1956; **5**:411–424.
21. Kestin J, Wang HE. Corrections for the oscillating disk viscometer. *Journal of Applied Mechanics* 1957; **24**:197–206.
22. Clark J, Kestin J, Shah VL. Effect of long-range intermolecular forces on the drag of an oscillating disk and on the viscosity of gases. *Physica A* 1977; **89**:539–554.
23. MacWood GE. The theory of the measurement of viscosity and slip of fluids by the oscillating disc method. *Physica* 1938; **5**:374–383.
24. MacWood GE. The theory of the measurement of viscosity and slip of fluids by the oscillating disc method, part II. *Physica* 1938; **5**:763–768.
25. Shah VL. Theory of the oscillating viscometer for slip flow. *Journal of Applied Mechanics* 1971; **38**:659–664.
26. Loyalka SK. Slip and jump coefficients for rarefied gas flows: Variational results for Lennard-Jones and $n(r)$-6 potential. *Physica A* 1990; **163**:813–821.
27. Maxwell JC. On stresses in rarefied gases arising from inequalities of temperature. *Royal Society—Philosophical Transactions A* 1879; **170**:231–256.
28. Barrat JL, Bocquet L. Large slip effect at nonwetting fluid–solid interface. *Physical Review Letters* 1999; **82**:4671–4674.
29. Hervet RPH, Leger L. Direct experimental evidence of slip in hexadecane: Solid interfaces. *Physical Review Letters* 2000; **85**:980–983.
30. Jeffery GB. On the steady rotation of a solid of revolution in a viscous fluid. *Proceedings of the London Mathematical Society* 1915; **14**:327–338.
31. Happel J, Brenner H. *Low Reynolds Number Hydrodynamics*. Prentice-Hall: Englewood Cliffs, New Jersey, 1965.
32. Loyalka SK. Theory of the spinning rotor gauge in the slip regime. *Journal of Vacuum Science and Technology A* 1996; **14**:2940–2945.
33. Tekasakul P, Bentz JA, Tompson RV, Loyalka SK. The spinning rotor gauge: Measurements of viscosity, velocity slip coefficients, and tangential momentum accommodation coefficients. *Journal of Vacuum Science and Technology A* 1996; **14**:2946–2952.

